Programmable bias field observed in graded ferromagnetic semiconductor films with broken symmetry

Sining Dong,[1,2,3] Yong-Lei Wang,[1,2,3] Seul-Ki Bac,[1,4] Xinyu Liu,[1,*] Vitalii Vlasko-Vlasov,[2] Wai-Kwong Kwok,[2] Sergei Rouvimov,[5] Sanghoon Lee,[4,†] Margaret Dobrowolska,[1] and Jacek K. Furdyna[1]

[1]*Department of Physics, University of Notre Dame, Notre Dame, Indiana 46556, USA*

[2]*Materials Science Division, Argonne National Laboratory, Argonne, Illinois 60439, USA*

[3]*Research Institute of Superconductor Electronics, School of Electronic Science and Engineering, Nanjing University, Nanjing 210093, China*

[4]*Physics Department, Korea University, Seoul 136-701, Republic of Korea*

[5]*Department of Electrical Engineering, University of Notre Dame, Notre Dame, Indiana 46556, USA*

(Received 18 March 2019; revised manuscript received 5 June 2019; published 19 July 2019)

We report on the observation of a field-induced magnetic bias effect in a $Ga_{0.94}Mn_{0.06}As_{1-y}P_y$ thin film with digitally graded phosphorus content. Although phosphorus concentration in the sample is changed in steps from $y \approx 0.03$ to $y \approx 0.28$, the magnetometry and magnetotransport data display a coherent magnetic response typical for single-layer in-plane magnetized films with cubic and weak [110] uniaxial anisotropy. Unexpectedly, low-temperature planar Hall resistance loops exhibit remarkable asymmetry tunable by application of strong in-plane initial magnetic field $H_{\rm Ini}$. We discuss this unusual memory effect, resembling the magnetization asymmetry in the exchange biased magnetic bilayers, in terms of a unidirectional bias field H_b induced by $H_{\rm Ini}$. We show that such bias field defines the delayed or accelerated nucleation of domains with chiral domain walls performing the magnetization reversal.

DOI: 10.1103/PhysRevMaterials.3.074407

I. INTRODUCTION

Broken inversion symmetry is an important source of a prominent spin-orbit coupling, unique magnetic order, and nonreciprocal effects in different crystal structures [1–3]. It can create new types of spin textures in noncentrosymmetric materials, such as noncollinear and frustrated magnetic phases [4,5] and magnetic skyrmions [6,7], promising novel magnetoelectric devices and magnetic memories. In semiconductor heterostructures, the broken inversion symmetry allows manipulation of the spin state through the voltage [8] and current [9], or induces the spin Hall effect [10], advancing new low-power spintronic applications. Among other materials showing strong spin-orbit interactions, ferromagnetic semiconductors (FMSCs) [11–13] offer a model system for developing and testing new tactics for controlling spins through symmetry breaking. Our earlier investigations of the FM-SCs focused on the control of the magnetization direction using current-induced spin-orbit torques [14–17]. In this work we pursue an alternative approach for designing magnetotransport properties and spin structures in the FMSCs by tuning the inversion symmetry in films with digitally graded composition and multiple interfaces. Such structural engineering enhances chiral effects, introduces tunable asymmetry in the magnetization reversal, and generates unusual domain-wall patterns.

Ferromagnetic semiconductors such as $Ga_{1-x}Mn_xAs$ are remarkable quantum materials, where a small amount of magnetic ions induces robust spin coherence in the system of delocalized holes, resulting in a typical ferromagnetic response [11–13]. Generally, $Ga_{1-x}Mn_xAs$ samples are grown using low-temperature molecular beam epitaxy (LTMBE), which allows precise control of the ion content and yields different equilibrium and even nonequilibrial crystal phases with user-defined atomic combination. Therefore, it is interesting to explore the ferromagnetic properties of $Ga_{1-x}Mn_xAs$-based alloys when their atomic compositions, and thus their physical properties, are graded along the growth direction creating a robust symmetry breaking along the film normal. In the present work, we thus study a unique anomalous effect in a quaternary alloy $Ga_{1-x}Mn_xAs_{1-y}P_y$ with composition graded along the film thickness and its relationship with the recently discovered chiral domain walls in such samples [18].

In the uniform $Ga_{1-x}Mn_xAs_{1-y}P_y$ films the presence of P leads to important consequences. First, it affects the exchange interaction between Mn ions, and thus the Curie temperature of the material [19,20]. Second, changing the lattice parameter automatically alters the strain in an epitaxial film due to lattice mismatch with the substrate, and thus modifies its magnetic anisotropy through the magnetoelastic coupling [21–24]. For example, the strain in uniform $Ga_{1-x}Mn_xAs_{1-y}P_y$ films grown on GaAs substrates changes from compressive to tensile with increasing the P content, y, forcing the orientation of the easy axis to change from in plane to out of plane.

In a graded $Ga_{1-x}Mn_xAs_{1-y}P_y$ film the gradient in P concentration should lead to a gradient of the energy gap, a gradient of strain, and thus also to a gradient of the concentration of holes that mediate the Mn-Mn exchange coupling. Importantly, variation of the lattice parameter along the compositional gradient will warranty the lack of the inversion

*Corresponding author: xliu2@nd.edu

†Corresponding author: slee3@korea.ac.kr

symmetry. One should expect that the above properties arising from the graded strain and composition will result in an entirely new magnetic system with novel ferromagnetic characteristics. In fact, in our earlier study [18] we found extreme asymmetry of the domain walls with respect to the easy axes, indicating that Dzyaloshinskii-Moriya interactions (DMIs), which have already been shown to play a prominent role in other diluted magnetic semiconductors [25], are strongly enhanced in such graded systems, while no heterogeneous features were observed in the macroscopic data. Here we demonstrate that the magnetization reversal, monitored by the magnetoresistance curves in our graded $Ga_{1-x}Mn_xAs_{1-y}P_y$ film, with a constant Mn concentration ($x \approx 0.06$) and the concentration of P varying in steps from $y \approx 0.03$ to $y \approx 0.28$ along the growth direction, exhibits a unique asymmetry induced by the application of a strong in-plane field. It is similar to the exchange bias effect observed in bilayers of dissimilar ferromagnetic materials, although our $\boldsymbol{M}(T)$ measurements and domain images reveal a strongly coupled magnetic state through the film thickness. We explain the observed asymmetry of the magnetization reversal in our film by memory effect causing a delayed or advanced growth of differently magnetized domains, which can be described equivalently by a tunable effective bias field defining history-dependent barriers for the domain nucleation in our multilayered sample.

II. EXPERIMENTS

$Ga_{1-x}Mn_xAs_{1-y}P_y$ samples were grown in a Riber 32 MBE system on semi-insulating GaAs (100) substrates using solid elemental sources of Ga and Mn evaporated from standard effusion cells. As and P were supplied by valved cracker cells, where both group-V elements were thermally cracked to produce dimer beam fluxes. An ionization flux gauge was used to calibrate the beam equivalent pressures and to monitor As and P concentration in the alloy. During the growth, the substrate temperature was kept constant, and the wafer was rotated in order to achieve a homogeneous composition in the film plane. The P concentration, y, along the growth direction was controlled by a mechanical valve equipped with a rapid flux control mechanism. Using a low substrate temperature (T_{Sub} of $\sim$250 °C) allowed us to optimize conditions for incorporating Mn. For grading the composition, the As_2/Ga flux ratio was kept constant ($\sim$10) during the entire growth, while the P_2 flux was changing in steps, with the P_2/As_2 flux ratio increasing from $\sim$0 to $\sim$1/2. The Mn flux was kept constant during the entire growth at a value corresponding to $x \approx 0.06$. The resulting multilayer was 100 nm thick and had eight $\sim$12.5-nm-thick sublayers, with y changing from 0.03 to $\approx$0.28 in steps of $\Delta y \sim 0.03 - 0.04$. The film growth was monitored by *in situ* reflection high-energy electron diffraction (RHEED). The RHEED patterns showed good two-dimensional surface morphology of the growing $Ga_{1-x}Mn_xAs_{1-y}P_y$, with (1×2) reconstruction at low values of the P flux, which changed to (1×1) reconstruction at higher P flux values ($y > 0.15$). The atomic concentrations in the film were examined by energy dispersive x-ray (EDX) microanalysis, which confirmed estimates made from the flux ratio and high-resolution x-ray diffraction (HRXRD) measurements using a Bruker D8 Discover high-resolution x-ray diffractometer.

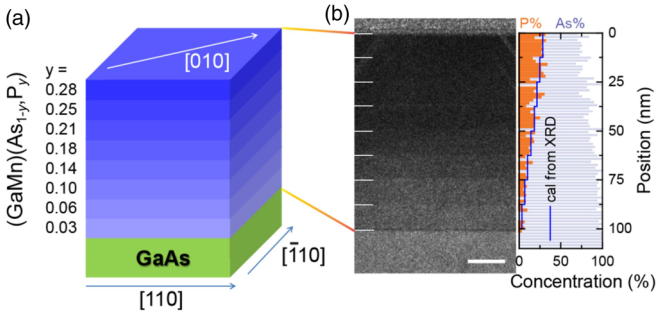

FIG. 1. Structure of the graded $Ga_{1-x}Mn_xAs_{1-y}P_y$ film. (a) Sketch of the eight-layer graded sample. (b) Dark-field TEM image of the sample cross section (the scale bar is 20 nm). EDX and XRD scans of the As and P concentrations are shown on the right of (b).

Temperature and field dependences of magnetization, M, of the graded $Ga_{0.94}Mn_{0.06}As_{1-y}P_y$ film were investigated using a Quantum Design MPMS XL superconducting quantum interference device (SQUID) magnetometer. For Hall effect measurement, a 1500(length) $\times$ 200(width) μm^2 Hall bar device with a long bridge along the [110] direction (effective area of the Hall voltage measurement $100 \times 200\,\mu m^2$) was patterned by photolithography and dry etching. The latter was performed in an inductive coupled plasma reactive ion setup using pure argon plasma milling at a rate of 2 nm/s. Electric contacts were covered with 20-nm Cr and 80-nm Au layers by electron beam evaporation.

The domain structure was visualized by a magneto-optical imaging technique using garnet indicator films with large Faraday rotation [26]. The graded $Ga_{1-x}Mn_xAs_{1-y}P_y$ samples were placed on the cold finger of the optical cryostat, covered with the indicator film, and studied in a polarized light microscope during the applied field cycling. The normal component of the stray fields (H_s) at emerging domain boundaries produced bright or dark contrast in the image, depending on the sign of H_s. It was captured with a digital camera and analyzed using image processing software.

III. RESULT AND DISCUSSION

A. Graded $Ga_{1-x}Mn_xAs_{1-y}P_y$ system

The structure of the graded $Ga_{0.94}Mn_{0.06}As_{1-y}P_y$ sample used in this investigation is sketched in Fig. 1(a). The film has eight 12.5-nm layers with successively increasing P concentration and sharp interfaces clearly resolved at the dark-field transmission electron microscopy (TEM) image in Fig. 1(b), which is sensitive to the elemental constituents and interfaces. The decreasing intensity of the TEM contrast corresponds to the increasing P concentration y from the bottom to the top of the sample, as also confirmed by the energy dispersive x-ray (EDX) and x-ray diffraction (XRD) analysis of P and As concentration [right of Fig. 1(b)]. The high-resolution TEM image showing the high quality of the film is presented in the Supplemental Material (see Fig. S1) [27].

The overall crystal integrity of the graded sample is further tested by high-resolution x-ray diffraction (HRXRD) measurements. Figure 2(a) shows 2θ-ω coupled diffraction scans

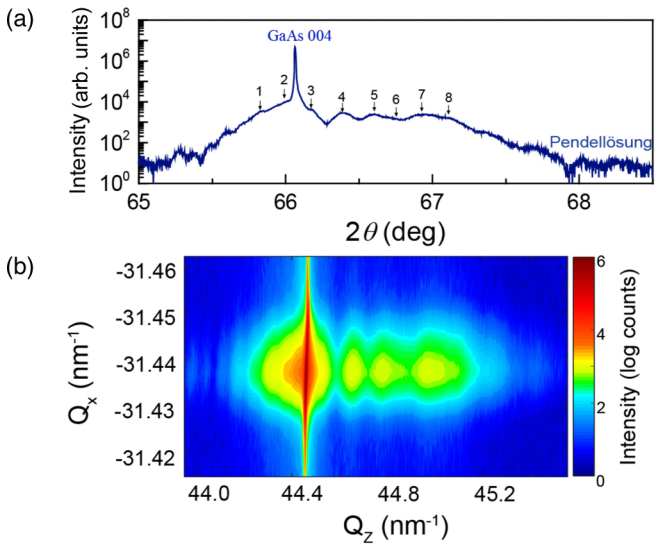

FIG. 2. HRXRD of the graded $Ga_{1-x}Mn_xAs_{1-y}P_y$ film. (a) XRD ω-2θ scan of the sample at GaAs (004) reflection. (b) The reciprocal space mapping of the sample (224) diffraction peaks.

measured along the growth direction [001]. The strongest peak located at 66.06° represents the (004) Bragg reflection of the GaAs substrate, while the series of weaker maxima are successive Bragg peaks of the $Ga_{0.94}Mn_{0.06}As_{1-y}P_y$ layers with different y. The increasing angle 2θ of the spectral maxima shows that the lattice constant along the growth direction decreases with a stepwise increase of the P concentration. This could be expected from studies of the single-layer films in a similar range of y [20].

Important features of the structure and strains in the graded multilayer are revealed by the reciprocal space mapping of the (224) diffraction peaks presented in Fig. 2(b). Here all eight peaks line up along a single Q_x line indicating that the constituent layers have the same unrelaxed in-plane lattice parameter. This means that with increasing the P concentration, the strains in the layers progress from compressive in the nearest to the substrate region to tensile in successive layers.

B. Magnetic and magnetotransport measurements

Figure 3(a) shows temperature dependences of magnetization $\boldsymbol{M}(T)$ in our film measured along the basic crystallographic directions upon warming, after application and switching off a large saturation field of 200 mT at 5 K. Remarkably, the graded multilayer sample demonstrates a strongly coupled magnetic response, revealing a single Curie temperature of ∼50 K, two in-plane easy axes (EA) close to [100] and [010] at low temperatures, and one in-plane EA along [$\bar{1}$10] at higher temperatures. This in-plane anisotropy is unexpected, since in single layers of $Ga_{1-x}Mn_xAs_{1-y}P_y$ grown directly on GaAs, the easy axis turns from in plane to out of plane at $y \gtrsim 0.10$ [23], well below the highest P concentration in our sample. The strongly coupled magnetic response is also surprising. It shows that the layers in our graded film are strongly coupled magnetically, which occurs because their thickness is smaller than the typical magnetic exchange length (∼17 nm) [18]. As a result, they behave as a single-layer film with in-plane magnetization, dominated by the layers close to the substrate, carrying a smaller P concentration, maximum density of the delocalized holes, and compressive strains. This conclusion is further verified by ferromagnetic resonance measurements of the multilayer sample, which reveal a single well-defined set of magnetic parameters, presented in the Supplemental Material (see Fig. S2) [27].

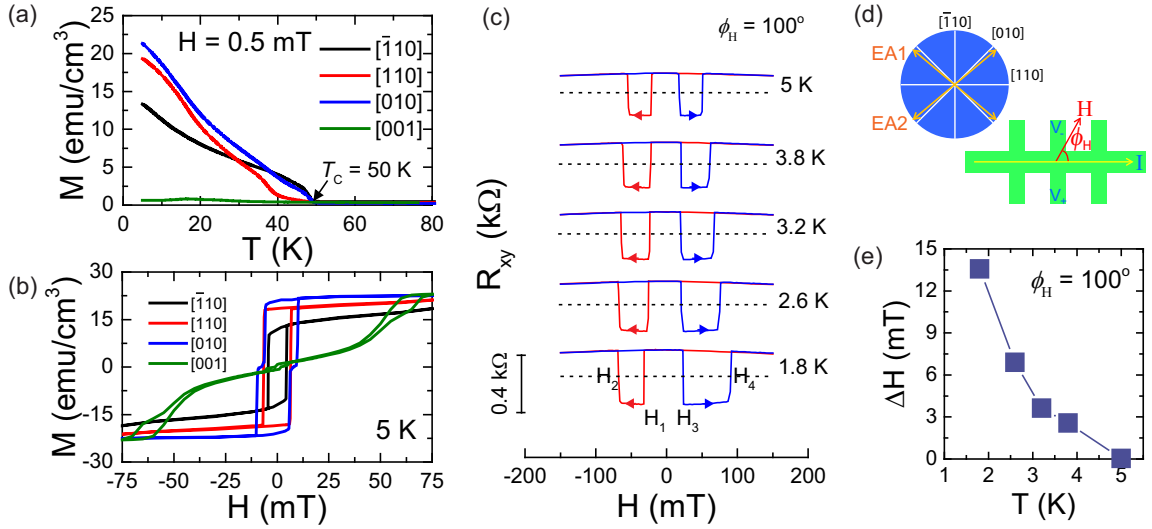

FIG. 3. Magnetic characterization of the graded $Ga_{1-x}Mn_xAs_{1-y}P_y$ film. (a) Temperature dependence of the remanent magnetization measured along principle axes during warming the sample after saturation by $H = 200$ mT at $T = 5$ K. (b) Hysteresis loops of the sample at 5 K. [100] curve (not shown) coincides with [010] curve. (c) Planar Hall resistance (PHR) traces measured in the in-plane field at $\phi_H = 100°$ after application of saturating field of 400 mT along the [010] direction. Blue and red curves represent the field sweeps in the positive and negative directions, respectively. The dashed lines show $R_{xy} = 0$. (d) Sketch of the bridge for the PHR measurements. (e) Temperature variations of the PHR curve asymmetry $\Delta H = (H_2 + H_4)/2$.

Similarly, the hysteresis $\boldsymbol{M}(\boldsymbol{H})$ loops measured at 5 K for different field orientations [Fig. 3(b)] reveal a single magnetic response with easy axes close to the in-plane ⟨100⟩ directions. Magnetization data measured at 2 and 3.5 K are presented in the Supplemental Material (see Fig. S3) [27]. According to sharp changes of the in-plane hysteresis loops at 2, 3.5, and 5 K, the magnetization reversal of the entire specimen occurs rapidly within ∼0.3–0.5 mT. As we show below, this happens through the domain nucleation and growth. The out-of-plane magnetization along the hard [001] axis goes much slower [green curve in Fig. 3(b)]. However, the normal saturation field $H_s||[001] \sim 70$ mT in our film is significantly smaller than in single layers of $Ga_{1-x}Mn_xAs$ with $x \approx 0.06$ where $H_s||[001]$ is >200 mT at 5 K. Obviously, the tensile strains in the top layers of our film soften the out-of-plane hard-axis behavior.

Temperature dependences of electrical resistivity and the first derivative of electrical resistivity of the graded $Ga_{1-x}Mn_xAs_{1-y}P_y$ film, as shown in the Supplemental Material (Fig. S4) [27], also indicate a strongly coupled magnetic response with $T_C \sim 50$ K. The increasing resistivity below 10 K suggests the nature of the carrier localization effect in the graded film. Moreover, Fig. 3(c) presents the planar Hall resistance (PHR) curves measured below 5 K in an in-plane magnetic field $\boldsymbol{H}$ swept at an angle $\phi_H = 100^\circ$ [see Fig. 3(d)] after application of a large initial field $H_{\rm Ini} = 400$ mT along the [010] axis ($\phi_{\rm Ini} = 45^\circ$). At $\phi_H = 100^\circ$, $\boldsymbol{H}$ is close to one of the hard axes, causing four magnetization switches within a ±200-mT field window. The curves in Fig. 3(c) reveal abrupt jumps of the PHR sign corresponding to ∼90° magnetization flips between two in-plane easy axes, which can be described by [28]

$$R_{\rm PHR} = (k/t)^2 \sin(2\phi_M). \quad (1)$$

Here t is the sample thickness, k is the anisotropic magnetoresistance ratio, and ϕ_M is the angle between magnetization and the current direction, [110]. With constant $k < 0$, Eq. (1) yields positive PHR when the magnetization is along one of the easy axes, at $\phi_M \sim 135^\circ$ (or 315°), and negative PHR for $\boldsymbol{M}$ along another easy axis at $\phi_M \sim 45^\circ$ (or 225°). The abruptness of the magnetization flips in Fig. 3(c) confirms again that our film behaves as a single exchange-coupled magnetic system rather than a series of different layers.

C. Magnetic memory effect in the graded structure

The PHR curves in Fig. 3(c) were measured after application and switching off the initial field $H_{\rm Ini}$ of 400 mT at $\phi_H = 45^\circ$ to [110]. At higher temperatures [$T > 3.8$ K in Fig. 3(c)] the effect of $H_{\rm Ini}$ is negligible, and the curves for opposite field sweeps are symmetric about $H = 0$, as is usually observed in single-layer $Ga_{1-x}Mn_xAs$ films [29]. However, at $T \lesssim 3.8$ K, they acquire a noticeable asymmetry, which increases with further cooling. It reveals different switching fields for the opposite field sweep directions. After application of the *negative* initial field $H_{\rm Ini} = -400$ mT, the asymmetric PHR curves flip horizontally around $H = 0$.

As a measure of the asymmetry we use a difference in the higher switching fields:

$$\Delta H = (H_4 + H_2)/2. \quad (2)$$

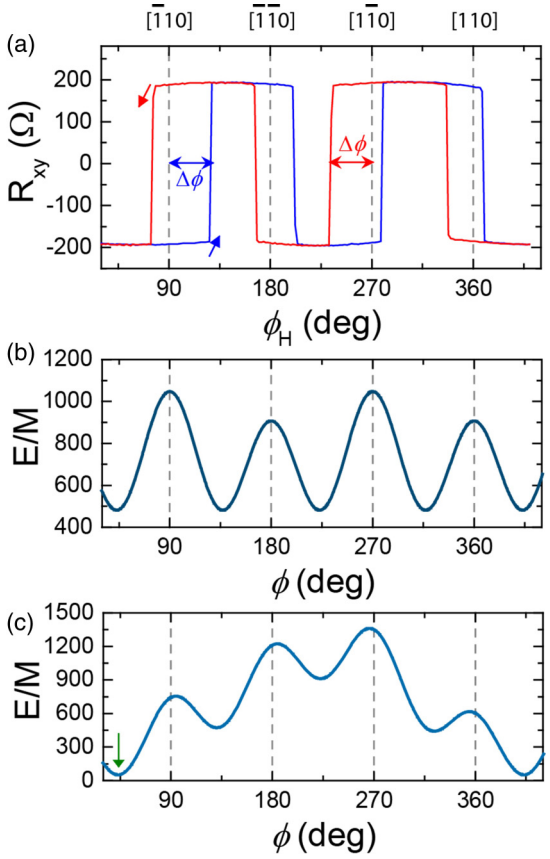

FIG. 4. (a) Angular variations of the planar Hall resistance in the rotating field of 50 mT at $T = 1.8$ K. The field was rotating counterclockwise (blue curve) and clockwise (red curve) after initial application of $H_{\rm Ini} = 800$ mT along [010]. (b) Angular dependence of the free energy $E(\phi)$ [Eq. (3)] with $H_b = 0$, and (c) $E(\phi)$ with $H_b = 11.0$ mT at an angle $\phi_b \sim 44.1^\circ$ from [110].

Here $H_4 > 0$ and $H_2 < 0$. The temperature changes of ΔH are shown in Fig. 3(e). Note that in single $Ga_{1-x}Mn_xAs$ layers, the PHR curves are always symmetric. Thus the asymmetry illustrated in Figs. 3(c) and 3(d) reveals a particular magnetic memory effect emerging in our multilayered sample. It resembles the exchange bias effect in bilayers of ferromagnetic films with different magnetic properties [30,31].

In our earlier study of $Ga_{1-x}Mn_xAs$ films we showed how the effective anisotropy field affects PHR curves measured in the rotating constant magnetic field [32,33]. Figure 4(a) presents similar rotating field measurements on our graded film after application of $H_{\rm Ini} = 800$ mT along [010]. The applied in-plane field of 50 mT was rotating counterclockwise (CCW) and then clockwise (CW) between 0° and 360° from the [110] axis at $T = 1.8$ K. The angular asymmetry between the CW (red) and CCW (blue) curves in Fig. 4(a) yields more evidence of the memory effect.

D. Bias field model

To understand the observed remagnetization asymmetry induced by $H_{\rm Ini}$ we used an expression for the free energy $E(\phi)$ of a magnetic film with two in-plane easy axes, and added a *unidirectional* anisotropy defining a bias field H_b oriented at

some angle ϕ_b in the film plane:

$$\frac{E}{M} = \frac{H_c}{8}\cos^2 2\phi + \frac{H_u}{2}\cos^2\phi - H_b\cos(\phi - \phi_b) - H\cos(\phi - \phi_H). \quad (3)$$

Here H is the external magnetic field; H_c and H_u are the cubic and uniaxial anisotropy fields. We assume that the effective bias field is generated by the application of a large $H_{\rm Ini}$ which polarizes the sample along $\sim\phi_b$. The angles ϕ, ϕ_H are the directions of $\boldsymbol{M}$ and the applied magnetic field $\boldsymbol{H}$ measured CCW from the [110] axis. In our experiment, the initial field, which imprints H_b, is along the [010] axis. So we admit that H_b is along the easy axis nearest to [010] where $\boldsymbol{M}$ points after switching off $H_{\rm Ini}$. It is slightly tilted (by $\sim 0.9°$ at $T = 1.8$ K) from [010] towards the uniaxial anisotropy axis [110].

Figures 4(b) and 4(c) compare the angular dependence of the free energy from Eq. (3) without the bias field, and with $H_b = 11.0$ mT at $\phi_b = 44.1°$ to [110]. Here we used $H_c = 249.0$ mT, $H_u = -7.3$ mT obtained by fitting the experimental data of angular PHR at large rotation fields for our sample at $T = 1.8$ K, as described in the Supplemental Material (Figs. S5 and S6) [27].

The steps in the $R_{xy}(\phi_H)$ traces correspond to the flips of $\boldsymbol{M}$ between the nearest minima of E. In the absence of H_b, the flip from $\sim$[010] ($\phi = 44.1°$) to $\sim[\bar{1}00]$ ($\phi = 135.9°$) during the CCW field rotation requires crossing the barrier at $[\bar{1}10]$ (90°), which will delay the flip. Similarly the reverse flip of $\boldsymbol{M}$ from $\sim[\bar{1}00]$ to $\sim$[010] during the CW rotation will be delayed by the same barrier. As a result there will be a hysteresis between CW and CCW PHR curves. However, as soon as the $[\bar{1}10]$ barrier is symmetric, the hysteresis should be also symmetric around $[\bar{1}10]$. The $[\bar{1}\bar{1}0]$ ($\phi = 180°$) barrier is lower and appropriate CW-CCW hysteresis will be narrower, but it will be also symmetric.

The situation changes if the bias field is present, as illustrated in Fig. 4(c). Now the CCW flip from $\sim$[010] to $\sim[\bar{1}00]$ [blue curve in Fig. 4(a)] will require crossing a larger barrier than for the reverse CW flip from $\sim[\bar{1}00]$ to $\sim$[010] [red curve in Fig. 4(a)]. As a result, the angular hysteresis will be asymmetric. The account of H_b makes all the barriers between the neighboring easy axes different for the CW and CCW rotation of $\boldsymbol{M}$. This yields four different flip conditions depending on the field rotation sign, as we see in the PHR curves of Fig. 4(a). Based on the asymmetry of flip angles from Fig. 4(a) we obtain $H_b \sim 11.0 \pm 0.5$ mT and $\phi_b \sim 44.1°$.

Figures 4(b) and 4(c) correspond to the coherent rotation of magnetization in the anisotropic magnetic potential with relatively large barriers between the equilibrium states. However, it was recognized long ago that the remagnetization can occur through the nucleation and growth of properly magnetized domains. The nucleation occurs across much weaker barriers formed at different structural defects. These small barriers can be explicitly introduced in the energy balance, as was done for analysis of the symmetric magnetization flips in thin biaxial Fe films [34]. Our *unidirectional* bias field H_b imitates an angular-dependent domain nucleation barrier that yields the asymmetric magnetization reversal.

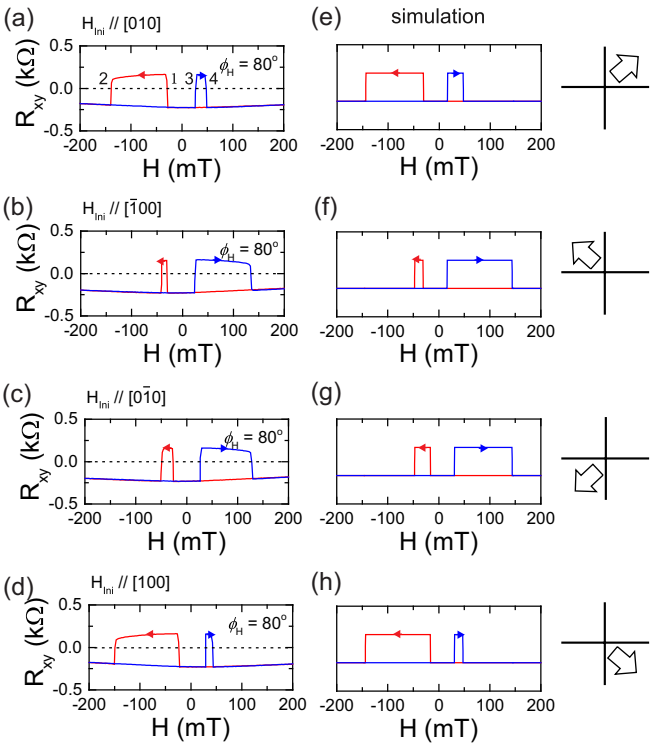

FIG. 5. Tuning the asymmetry of the magnetization reversal by the orientations of $H_{\rm Ini}$. (a)–(d) PHR curves measured at $\phi_H = 80°$ after application of $H_{\rm Ini} = 400$ mT along four different ⟨100⟩ directions at $T = 1.8$ K. (e)–(h) PHR curves calculated using the bias field $H_b = 11.0$ mT aligned with the sample easy axes as shown in the right column. Blue and red curves show opposite field sweeps, up and down, respectively.

E. Dependence of the bias field on $H_{\rm Ini}$

To clarify the dependence of H_b on the initial field $H_{\rm Ini}$, we have measured PHR curves after application of differently oriented $H_{\rm Ini}$ and sweeping H in the same direction (see Fig. S7 in the Supplemental Material) [27]. Comparison of the PHR loops shows that their asymmetry changes sign as the angle of $H_{\rm Ini}$ passes the direction of the hard axes in accordance with changes of the initial $\boldsymbol{M}$ orientation after switching off $H_{\rm Ini}$. Most interestingly, such repeating pattern suggests H_b, defined by the asymmetry, is imprinted along the easy axis by $H_{\rm Ini}$ every time the angle of $H_{\rm Ini}$ passes one of four easy directions. To confirm such distinct relation, Figs. 5(a)–5(d) present PHR curves at $T = 1.8$ K for four different orientations of $H_{\rm Ini}$ close to easy axes of the film as shown by arrows in the right column of the figure. To simplify the analysis, they were all measured at the same $\phi_H = 80°$. Corresponding PHR curves calculated for this sweep angle using $H_b = 11.0$ mT in Eq. (3) are plotted in Figs. 5(e) and 5(f). Close agreement between the measured and simulated PHR traces confirms the validity of our bias field model and the distinct relationship between H_b and $H_{\rm Ini}$.

Below we show how the bias field H_b depends on the magnitude of $H_{\rm Ini}$. Assuming that this dependence is hysteretic we carried out experiments commonly used for analyzing details of the hysteresis loops. After application of a large saturation field $H_{\rm Ini}$ of 800 mT in a chosen direction, a smaller field

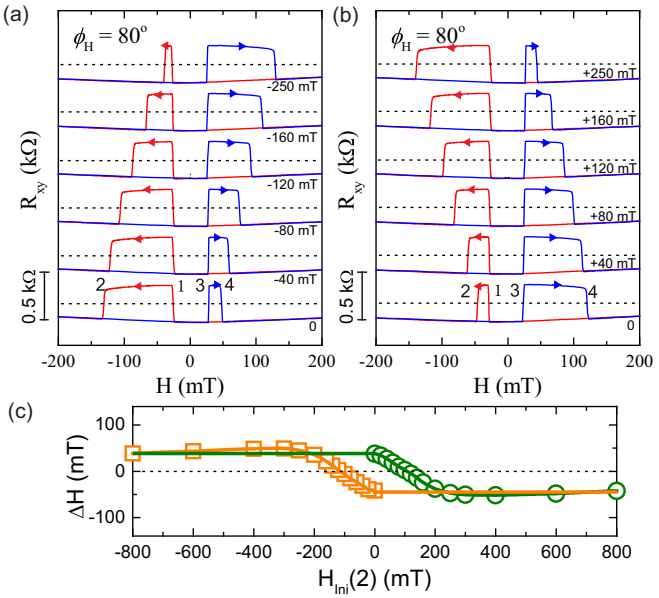

FIG. 6. Dependence of the magnetization reversal asymmetry on the strength of $H_{\rm Ini}$. After a large saturation field of 800 mT along [010] and application of different opposite fields $H_{\rm Ini(2)}$, the field is swept between ±200 mT at $\phi_H = 80^\circ$ at $T = 1.8$ K. In (a) the PHR curves are measured after $H_{\rm Ini} = 800$ mT and $H_{\rm Ini(2)}$ changing from 0 to −250 mT, and in (b) after $H_{\rm Ini} = -800$ mT and $H_{\rm Ini(2)}$ increasing from 0 to +250 mT. Corresponding $H_{\rm Ini(2)}$ values are shown in the panels. (c) The asymmetry parameter ΔH [Eq. (2)] for different $H_{\rm Ini(2)}$.

$H_{\rm Ini(2)}$ was applied in the opposite direction and switched off. Then the PHR curves were measured in a narrow range of the sweeping field (±200 mT) at $\phi_H = 80^\circ$. A series of PHR curves obtained after different $H_{\rm Ini(2)}$, which maps out the H_b-$H_{\rm Ini}$ relation, is shown in Figs. 6(a) and 6(b).

In Fig. 6(c) we plot the asymmetry parameter ΔH defined by Eq. (2), which corresponds to the unidirectional bias field changing with $H_{\rm Ini}$. It shows that the remagnetization asymmetry gradually decreases with increasing the inverse field $H_{\rm Ini(2)}$ and changes sign at $|H_{\rm Ini(2)}| \sim 120$ mT. Clearly, the inverse field $H_{\rm Ini(2)}$ smoothly wipes out the history of the large $H_{\rm Ini}$ and at $|H_{\rm Ini(2)}| > 250$ mT the memory effect saturates. The dependence of ΔH on $H_{\rm Ini}$ shows a possibility of the precise control of the remagnetization process asymmetry by changing the direction and the strength of the initial field.

F. Domain evolution in graded $Ga_{1-x}Mn_xAs_{1-y}P_y$ multilayer

As was shown in our recent paper [18], the magnetization of the graded multilayer switches through the nucleation and fast growth of differently polarized domains. Figure 7 demonstrates typical domain structure patterns emerging near the switching field at 3.8 K. The sample was initially polarized by the field of 210 mT along [$\bar{1}$00] (close to one of the easy axes), and then the field is swept in the opposite [100] direction in small increments of 0.06 mT. Figure 7 illustrates the second flip of magnetization from the [0$\bar{1}$0] [red arrow in Figs. 7(a)–7(d)] into the [100] state (green arrow). New domains appear [Fig. 7(b)] and rapidly grow in a narrow field window ∼0.6 mT [Figs. 7(c) and 7(d)], until the entire sample is magnetized along [100] [Fig. 7(e)]. Cycling the field reveals four similar domain nucleation and growth events (see Fig. S8 in the Supplemental Material) [27], corresponding to the four sharp steps in the PHR curves.

Remarkably, the domain walls in Fig. 7 are perfectly aligned with the easy axes of the sample. They form rhombic patterns due to the presence of a small uniaxial [110] anisotropy slightly tilting the easy axes from the in-plane ⟨100⟩ directions. The ultimate asymmetry of nearly 90° domain walls parallel to the easy axes is a unique feature of the studied multilayered sample. It results from the DMIs enhanced by the presence of multiple interfaces and the compositional gradient, as discussed in detail in Ref. [18].

The chiral anisotropy introduced by the DMI could also cause the variation of the domain nucleation barriers responsible for the memory effect. Application of a strong magnetic field polarizes magnetic moments around domain nucleation

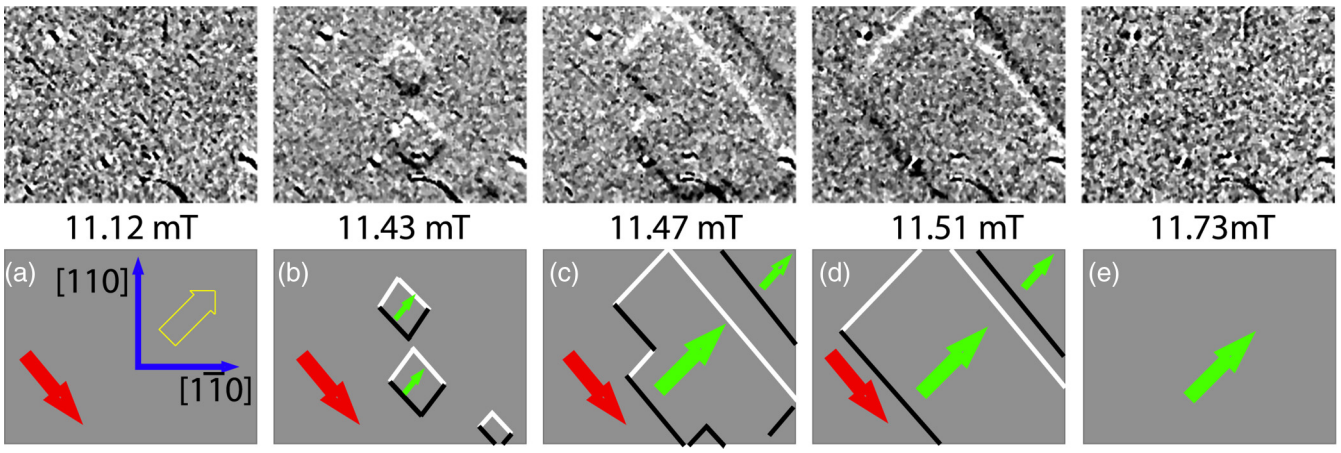

FIG. 7. Nucleation and expansion of magnetic domains in the graded $Ga_{1-x}Mn_xAs_{1-y}P_y$ film at $T = 3.8$ K. In (a) the sample is polarized along the easy axis close to [0$\bar{1}$0] (red arrow) and the domain images are captured in the increasing field H‖[100] (yellow open arrow). Field values are shown under the images. Bright and dark contrast reveals up and down stray fields induced by positive and negative magnetic charges at the domain walls. The easy axis in the emerging domains is shown by the green arrow. The frame size is 350 μm × 450 μm.

centers. In turn, due to the DMI, the local rotation of $\boldsymbol{M}$, which seeds emerging new domains, can be either delayed or accelerated causing the asymmetry in the transitions between different easy axes.

IV. CONCLUDING REMARKS

The observed remagnetization asymmetry in our multilayered film exposes an intriguing memory effect induced by a strong in-plane magnetic field. It can be described by a unidirectional bias field H_b emerging in addition to the cubic and uniaxial anisotropy fields, that are usually present in single-layer $Ga_{1-x}Mn_xAs_{1-y}P_y$ films. Remarkably, the low-temperature value of H_b obtained from the fitting of different experimental PHR curves is the same (11.0 mT at $T = 1.8$ K), and the direction of $\boldsymbol{H}_b$ is always imprinted along one of the easy magnetization axes. However, H_b rapidly decreases with increasing temperature, and at $T = 5$ K the remagnetization asymmetry disappears. At $T < 4$ K the field $H_{\rm Ini} \sim 250$ mT (slightly larger than the cubic anisotropy field) is sufficient for inducing maximum H_b. This allows simple reprogramming of the bias field using the initial polarization of the sample along one of the easy axes.

Noting that the observed asymmetry in the PHR flips may correspond to the shift in the domain nucleation fields, we ascribe it to the local spin structure at domain nucleation centers, which is changed by $H_{\rm Ini}$. New domains appear by rotation of spins from this local state to a neighboring easy axis. Clearly this process will depend on the local spin polarization induced by $H_{\rm Ini}$ and on the subsequent sweeping field direction.

We must emphasize here that, although the existence of Mn interstitials and nanoclusters (which serve as nucleation centers potentially) in all GaMnAs films is common, formation of a unidirectional bias field presently reported is never observed in GaMnAs and GaMnAsP films where there is no graded composition. We have no theoretical explanation of how graded composition of the material leads to the observed unidirectional bias field. In this connection we note, however, that in an earlier paper on the graded $Ga_{1-x}Mn_xAs_{1-y}P_y$ system (Ref. [18]) some of us have reported a unique behavior of magnetic domains that has been ascribed to the possible presence of broken inversion symmetry and DMIs. It is on that basis that we speculate that the chiral DMI coupling, which defines the unusual Néel wall structure in our samples [18], may be one of the factors causing the remagnetization asymmetry. Depending on the sense of rotation (CW or CCW) of the local spins at the nucleation center towards the applied field, it can delay or accelerate the new domain nucleation. It has been already shown that DMI initiates the exchange bias in IrMn3/Co [35], causes asymmetric domain-wall motion in Pt/Co/Pt [36], and results in the asymmetric hysteresis in Pt/Co/Ir [37] films with perpendicular anisotropy. Compared to the normal anisotropy case, the effect of DMI in our in-plane magnetized films is more intricate. However, if the normal component of magnetization emerges during the domain nucleation, opposite twists of $\boldsymbol{M}$ become clearly unequal [18].

The sturdy domain-wall orientation along the easy axes in the graded DMI samples yields robust consistency of their motion. This may be important for stability of current-driven domain-wall devices [38]. In turn, the domain-wall chirality may significantly reduce critical currents required for moving the domain walls [39,40]. The observed tunable bias effect causing the nucleation and expansion of precisely shaped domains in the graded DMI multilayers may therefore be of interest in designing alternative domain-wall-based programmable spintronic devices.

ACKNOWLEDGMENTS

The work at University of Notre Dame was supported by the NSF Grant No. DMR14-00432. The work at Argonne National Laboratory was supported by the U.S. Department of Energy, Office of Science, Materials Sciences and Engineering Division. The work at Nanjing University was supported by National Natural Science Foundation of China (Grants No. 61771235 and No. 61727805) and the National Key R&D Program of China (2018YFA0209002). The work at Korea University was supported by Basic Science Research Program through the National Research Foundation of Korea (NRF) funded by the Ministry of Education (2018R1D1A1A02042965) and by Ministry of Science ICT (2018R1A4A1024157). We appreciate constructive comments and suggestions from Ulrich Welp, Xiang Li, and Taehee Yoo. The data that support the findings of this study are available from the corresponding authors upon reasonable request.

[1] J. Fabian, A. Matos-Abiague, C. Ertler, P. Stano, and I. Žutić, Semiconductor spintronics, Acta Phys. Slovaca **57**, 565 (2007).

[2] Y. Xu, D. D. Awschalom, and J. Nitta, *Handbook of Spintronics* (Springer, Dordrecht, Netherlands, 2015).

[3] M. S. Dresselhaus, G. Dresselhaus, and A. Jorio, *Group Theory: Application to the Physics of Condensed Matter* (Springer, Berlin-Heidelberg, 2008).

[4] T. Kimura, J. C. Lashley, and A. P. Ramirez, Inversion-symmetry breaking in the noncollinear magnetic phase of the triangular-lattice antiferromagnet $CuFeO_2$, Phys. Rev. B **73**, 220401(R) (2006).

[5] S.-W. Cheong and M. Mostovoy, Multiferroics: A magnetic twist for ferroelectricity, Nat. Mater. **6**, 13 (2007).

[6] S. Seki, X. Yu, S. Ishiwata, and Y. Tokura, Observation of skyrmions in a multiferroic material, Science **336**, 198 (2012).

[7] Y. Nii, T. Nakajima, A. Kikkawa, Y. Yamasaki, K. Ohishi, J. Suzuki, Y. Taguchi, T. Arima, Y. Tokura, and Y. Iwasa, Uniaxial stress control of skyrmion phase, Nat. Commun. **6**, 8539 (2015).

[8] F. Matsukura, Y. Tokura, and H. Ohno, Control of magnetism by electric fields, Nat. Nanotechnol. **10**, 209 (2015).

[9] A. Manchon, J. Zelezný, I. M. Miron, T. Jungwirth, J. Sinova, A. Thiaville, K. Garello, and P. Gambardella, Current-induced spin-orbit torques in ferromagnetic and antiferromagnetic systems, arXiv:1801.09636.

[10] J. Sinova, S. O. Valenzuela, J. Wunderlich, C. H. Back, and T. Jungwirth, Spin hall effects, Rev. Mod. Phys. **87**, 1213 (2015).

[11] T. Dietl and H Ohno, Dilute ferromagnetic semiconductors: Physics and spintronic structures, Rev. Mod. Phys. **86**, 187 (2014).

[12] T. Jungwirth, J. Wunderlich, V. Novák, K. Olejník, B. L. Gallagher, R. P. Campion, K. W. Edmonds, A. W. Rushforth, A. J. Ferguson, and P. Němec, Spin-dependent phenomena and device concepts explored in (Ga, Mn)As, Rev. Mod. Phys. **86**, 855 (2014).

[13] M. Tanaka, S. Ohya, and P. Nam Hai, Recent progress in III-V based ferromagnetic semiconductors: Band structure, Fermi level, and tunneling transport, Appl. Phys. Rev. **1**, 011102 (2014).

[14] A. Chernyshov, M. Overby, X. Liu, J. K. Furdyna, Y. Lyanda-Geller, and L. P. Rokhinson, Evidence for reversible control of magnetization in a ferromagnetic material by means of spin–orbit magnetic field, Nat. Phys. **5**, 656 (2009).

[15] S. Lee, S. Choi, S.-K. Bac, K. J. Lee, J. Chang, S. Choi, P. Chongthanaphisut, S. Lee, X. Liu, M. Dobrowolska, and J. K. Furdyna, Determination of current-induced spin-orbit effective magnetic field in GaMnAs ferromagnetic semiconductor, Appl. Phys. Lett. **111**, 252401 (2017).

[16] S. Lee, S. Lee, S.-K. Bac, S. Choi, X. Liu, M. Dobrowolska, and J. K. Furdyna, Spin–Orbit-Induced Effective Magnetic Field in GaMnAs Ferromagnetic Semiconductor, IEEE Trans. Magn. **55**, 1 (2019).

[17] S. Lee, T. Yoo, S.-K. Bac, S. Choi, H. Lee, S. Lee, X. Liu, J. K. Furdyna, and M. Dobrowolska, Manipulation of magnetization in GaMnAs films by spin-orbit-induced magnetic fields, Curr. Appl. Phys. **17**, 801 (2017).

[18] V. K. Vlasko-Vlasov, W.-K. Kwok, S. Dong, X. Liu, M. Dobrowolska, and J. K. Furdyna, Extreme asymmetry of Néel domain walls in multilayered films of the dilute magnetic semiconductor (Ga,Mn)(As,P), Phys. Rev. B **98**, 180411(R) (2018).

[19] W. Ouerghui, H. B. Abdallah, and K. B. Saad, First-principles calculations on magnetism and exchange interactions in GaMnAs and GaMnAsP, Phys. Status Solidi B **254**, 1700115 (2017).

[20] X. Li, X. Liu, S. Dong, C. Gorsak, J. K. Furdyna, and M. Dobrowolska, Dependence of ferromagnetic properties on phosphorus concentration in $Ga_{1-x}Mn_xAs_{1-y}P_y$, J. Vac. Sci. Technol., B **36**, 02D104 (2018).

[21] A. Lemaître, A. Miard, L. Travers, O. Mauguin, L. Largeau, C. Gourdon, V. Jeudy, M. Tran, and J.-M. George, Strain control of the magnetic anisotropy in (Ga, Mn)(As, P) ferromagnetic semiconductor layers, Appl. Phys. Lett. **93**, 021123 (2008).

[22] M. Cubukcu, H. J. von Bardeleben, Kh. Khazen, J. L. Cantin, O. Mauguin, L. Largeau, and A. Lemaître, Adjustable anisotropy in ferromagnetic (Ga, Mn)(As, P) layered alloys, Phys. Rev. B **81**, 041202(R) (2010).

[23] X. Liu, X. Li, S.-K. Bac, X. Zhang, S. Dong, S. Lee, M. Dobrowolska, and J. K. Furdyna, Ferromagnetic resonance and spin-wave resonances in GaMnAsP films, AIP Adv. **8**, 056402 (2018).

[24] T. Niazi, M. Cormier, D. Lucot, L. Largeau, V. Jeudy, J. Cibert, and A. Lemaître, Electric-field control of the magnetic anisotropy in an ultrathin (Ga,Mn)As/(Ga,Mn)(As,P) bilayer, Appl. Phys. Lett. **102**, 122403 (2013).

[25] N. Samarth and J. K. Furdyna, Electron paramagnetic resonance in $Cd_{1-x}Mn_xS$, $Cd_{1-x}Mn_xSe$, and $Cd_{1-x}Mn_xTe$, Phys. Rev. B **37**, 9227 (1988).

[26] V. K. Vlasko-Vlasov, G. W. Crabtree, U. Welp, and V. I. Nikitenko, Magneto-optical studies of magnetization processes in high-Tc superconductors, NATO ASI Ser., Ser. E **356**, 205 (1999).

[27] See Supplemental Material at http://link.aps.org/supplemental/10.1103/PhysRevMaterials.3.074407 for more information.

[28] H. Tang, R. Kawakami, D. Awschalom, and M. Roukes, Giant Planar Hall Effect in Epitaxial (Ga, Mn) As Devices, Phys. Rev. Lett. **90**, 107201 (2003).

[29] D. Y. Shin, S. J. Chung, S. Lee, X. Liu, and J. K. Furdyna, Stable Multidomain Structures Formed in the Process of Magnetization Reversal in GaMnAs Ferromagnetic Semiconductor Thin Films, Phys. Rev. Lett. **98**, 047201 (2007).

[30] J. Nogués and I. K Schuller, Exchange bias, J. Magn. Magn. Mater. **192**, 203 (1999).

[31] A. Berkowitz and K. Takano, Exchange anisotropy—a review, J. Magn. Magn. Mater. **200**, 552 (1999).

[32] J. Won, J. Shin, S. Lee, T. Yoo, H. Lee, S. Lee, X. Liu, and J. Furdyna, Temperature behavior of uniaxial anisotropy along [100] direction in GaMnAs films, Appl. Phys. Express **6**, 013001 (2012).

[33] J. Kim, S. Lee, S. Lee, X. Liu, and J. Furdyna, Investigation of domain pinning fields in ferromagnetic GaMnAs films using angular dependence of the planar Hall effect, Solid State Commun. **150**, 27 (2010).

[34] R. P. Cowburn, S. J. Gray, J. Ferré, J. A. C. Bland, and J. Miltat, Magnetic switching and in-plane uniaxial anisotropy in ultrathin Ag/Fe/Ag(100) epitaxial films, J. Appl. Phys. **78**, 7210 (1995).

[35] R. Yanes, J. Jackson, L. Udvardi, L. Szunyogh, and U. Nowak, Exchange Bias Driven by Dzyaloshinskii-Moriya Interactions, Phys. Rev. Lett. **111**, 217202 (2013).

[36] S.-G. Je, D.-H. Kim, S.-C. Yoo, B.-C. Min, K.-J. Lee, and S.-B. Choe, Asymmetric magnetic domain-wall motion by the Dzyaloshinskii-Moriya interaction, Phys. Rev. B **88**, 214401 (2013).

[37] D.-S Han, N.-H. Kim, J.-S. Kim, Y. Yin, J.-W. Koo, J. Cho, S. Lee, M. Kläui, H. J. M. Swagten, B. Koopmans, and C.-Y. You, Asymmetric hysteresis for probing Dzyaloshinskii–Moriya interaction, Nano Lett. **16**, 4438 (2016).

[38] A. Thiaville, S. Rohart, É. Jué, V. Cros, and A. Fert, Dynamics of Dzyaloshinskii domain walls in ultrathin magnetic films, EPL **100**, 57002 (2012).

[39] O. A. Tretiakov and A. Abanov, Current Driven Magnetization Dynamics in Ferromagnetic Nanowires with a Dzyaloshinskii-Moriya Interaction, Phys. Rev. Lett. **105**, 157201 (2010).

[40] K.-S. Ryu, L. Thomas, S.-H. Yang, and S. Parkin, Chiral spin torque at magnetic domain walls, Nat. Nanotechnol. **8**, 527 (2013).